Reproductive Toxicology 64 (2016) 151–161

Contents lists available at ScienceDirect

Reproductive Toxicology

journal homepage: www.elsevier.com/locate/reprotox

Computational modeling and simulation of genital tubercle development

Maxwell C.K. Leung[a,b,*], M.Shane Hutson[b,c], Ashley W. Seifert[d], Richard M. Spencer[e], Thomas B. Knudsen[a,*]

[a] National Center for Computational Toxicology, U.S. Environmental Protection Agency, Research Triangle Park, NC, 27711, United States
[b] Oak Ridge Institute for Science and Education, Oak Ridge, TN, 37831, United States
[c] Department of Physics & Astronomy, Vanderbilt Institute for Integrative Biosystems Research & Education, Vanderbilt University, Nashville, TN, 37235, United States
[d] Department of Biology, University of Kentucky, Lexington, KY, 40506, United States
[e] Lockheed Martin, Research Triangle Park, NC, 27709, United States

ARTICLE INFO

Article history:
Received 10 February 2016
Received in revised form 13 April 2016
Accepted 7 May 2016
Available online 11 May 2016

Keywords:
Agent-based model
Genital tubercle
Hypospadias
Computational toxicology

ABSTRACT

Hypospadias is a developmental defect of urethral tube closure that has a complex etiology involving genetic and environmental factors, including anti-androgenic and estrogenic disrupting chemicals; however, little is known about the morphoregulatory consequences of androgen/estrogen balance during genital tubercle (GT) development. Computer models that predictively model sexual dimorphism of the GT may provide a useful resource to translate chemical-target bipartite networks and their developmental consequences across the human-relevant chemical universe. Here, we describe a multicellular agent-based model of genital tubercle (GT) development that simulates urethrogenesis from the sexually-indifferent urethral plate stage to urethral tube closure. The prototype model, constructed in CompuCell3D, recapitulates key aspects of GT morphogenesis controlled by SHH, FGF10, and androgen pathways through modulation of stochastic cell behaviors, including differential adhesion, motility, proliferation, and apoptosis. Proper urethral tube closure in the model was shown to depend quantitatively on SHH- and FGF10-induced effects on mesenchymal proliferation and epithelial apoptosis—both ultimately linked to androgen signaling. In the absence of androgen, GT development was feminized and with partial androgen deficiency, the model resolved with incomplete urethral tube closure, thereby providing an *in silico* platform for probabilistic prediction of hypospadias risk across combinations of minor perturbations to the GT system at various stages of embryonic development.

1. Introduction

Alterations in male urological development may be invoked by genetic errors and/or chemical disruption at critical times during embryo-fetal development, leading to clinical conditions such as microphallus (micropenis), chordee, and hypospadias [1–3]. Hypospadias is a neotenous defect in urethral tube closure during male genital tubercle (GT) development, resulting in one of the most common human birth defects (1 case per 200–300 liveborn males) [4,5]. The developmental origins of hypospadias encompass embryonic stages during which the sexually indifferent GT primordium is specified and then patterned into male or female phenotypes [6,7]. Male GT development, as for most embryology, is composed of many interacting parts (molecules, cells, tissues) in an intricate arrangement. As such, GT specification, patterning, and differentiation are precisely orchestrated by genetic pathways and cellular processes. Networks of individual interactions ultimately govern how the system behaves in response to chemical-induced perturbation. Multiscale modeling and simulation are thus an important approach for discovery and synthesis of biological

Abbreviations: AR, androgen receptor; ARE, androgen response element; BMP, bone morphogenetic protein; CM, core mesenchyme; EC, ectoderm; ECM, extracellular matrix; eUPE, excluded urethral plate endoderm; FGF10, fibroblast growth factor 10; GT, genital tubercle; HTS, high-throughput screening; LM, lumen; MCS, Monte Carlo steps; PM, preputial mesenchyme; RAR, retinoic acid receptor; RXR, retinoid X receptor; SHH, sonic Hedgehog; UPE, urethral plate endoderm; UTDs, urethral Tube Closure Defects; WNT, wingless-int.

* Corresponding authors at: U.S. Environmental Protection Agency, 109 T.W. Alexander Drive, Research Triangle Park, NC 27711, United States.
E-mail addresses: leung.maxwell@epa.gov (M.C.K. Leung), knudsen.thomas@epa.gov (T.B. Knudsen).

http://dx.doi.org/10.1016/j.reprotox.2016.05.005
0890-6238/

design principles underlying the response of complex adaptive systems to perturbation. Such is the case for developmental toxicity.

Our capacity to predict adverse developmental outcomes in a complex adaptive system utilizing computational (*in silico*) models may be advanced by knowledge-driven architectures of cellular networks that are both dynamic in their control and resilient in their response to chemical-induced perturbation. Prior to sexual differentiation, GT development is directed by a number of signaling pathways, including SHH/IHH, FGF, BMP, HOX, WNT, RAR/RXR, and ephrin/EphB2 [3,8–15]. Subsequently, the GT develops into a male or female phenotype depending on androgen production from the fetal testis [16–19] and estrogen production from maternal and other sources [20–23]. In human populations, an increased risk of hypospadias has been associated with single nucleotide polymorphisms (SNPs) in the SHH and FGF pathways [24,25]. In mouse genetic models, hypospadias has been linked to functional inactivation of morphoregulatory pathways such as SHH-FGF10 signaling [10,16] and to disruption of androgen synthesis/signaling. The latter follows from prenatal exposure to environmental chemicals that may alter endocrine balance in the developing fetus, such as bisphenol A, flutamide, phthalates, and vinclozolin [26–28]. Although disruption of androgen-responsive pathways is a primary cause of hypospadias [29–31], knocking out morphogenetic signaling pathways such as SHH/IHH or FGF10 in mice causes profound changes in GT development, including changes in epithelial structure [32], suppression of mesenchymal proliferation, and the distribution of programmed cell death (apoptosis) [3,10,16,18]. Still, relatively little is known about the morphoregulatory consequences of androgen/estrogen balance during GT development [3,32–35].

Earlier investigations have highlighted some of the interplay between androgen/estrogen balance, morphoregulatory signals, and cellular behaviors underlying the patterning and sexual dimorphism of GT development. For example, normal urethral development in male embryos requires closure and separation of the urethral plate endoderm from the overlying ectoderm on the ventral surface of the GT. This process is linked to sexually-dimorphic patterns of programmed cell death (apoptosis) and the local regulation of mesenchymal cell proliferation by signaling pathways such as hedgehog (SHH/IHH), FGF (FGF8, FGF10), WNT and BMP [3,35–38]. Other investigations have focused on the integration of functional genetics and epidemiology [1,2,29,33,39–42]. These are primarily qualitative models that detail the mechanisms of GT development based on functional tests of specific molecular pathways, but they lack predictive power. None provides a quantitative platform for evaluating hypotheses and generating experimentally testable predictions.

Previously, we used a systems toxicology approach [43] to identify significant correlations between environmental chemicals, molecular targets, and adverse outcomes across a broad chemical landscape with emphasis on developmental toxicity of the male reproductive system in the ToxCast library [44]. That study demonstrated a phenotypic hierarchy of testicular atrophy, sperm effects, tumors, and malformations that, in composite resembled the human Testicular Dysgenesis Syndrome (TDS) [45]. A subset of 54 chemical compounds with male developmental consequences had *in vitro* bioactivity on molecular targets that could be condensed into 156 gene annotations in a 'chemical-target bipartite network'. Although hypospadias was only one endpoint in the study, the model supported the known role of androgen and estrogen signaling pathways in the TDS hypothesis and expanded the list of molecular targets to include vascular remodeling proteins, G-protein coupled receptors (GPCRs), cytochrome-P450s, and retinoic acid signaling [44].

Given the biological complexity of GT development, computer models that predictively model sexual dimorphism of the GT may provide a useful resource to translate chemical-target bipartite networks and their developmental consequences across the human-relevant chemical universe. Here, we (i) construct a multicellular agent-based model (ABM) of GT development based on available biological information, (ii) evaluate the model's performance in recapitulating cellular changes underlying urethral tube closure, and (iii) use the model to examine how the interplay between SHH, FGF10, and androgen signaling is disrupted in urethral closure defects. The ABM simulates the actions and interactions of autonomous agents (cells) in a shared environment to assess their quantitative effects on the system as a whole. These models can distinguish key events leading to structural malformations, identify moments in development at which interventions have extreme consequences, and use systematic parameter sweeps to rank order system sensitivities [46–48]. The simulations make hypotheses and assumptions explicit for 'what-if' and 'what happens next' questions that can help inform predictive toxicology.

2. Methods and implementation

2.1. Scope of the GT model

A major challenge to systems-level simulation of GT development is defining an appropriately abstracted model and boundary conditions. One key genetic model for the study of biochemical signaling in GT development has been the mouse [10,16,32,35–38,49–52]. Gestational days E12.5 to E19.5 encompass the sequence of morphogenetic events from the urogenital sinus stage to formation of the urethral canal and distal opening. These events fashion GT development anatomically by temporal and spatial (proximo-distal) progression of cellular changes that are sensitive to fetal testosterone production, commencing at E15.5 after the onset of steroidogenesis during the Male Programming Window (MPW) from E14.5 to E.16.5 (as extrapolated from E16.5 to E18.5 in rats [53,54]). The period from E12.5 to E19.5 also encompasses the window of vulnerability to both sexual dimorphism and hypospadias in this species. Within this window, environmental disruptions invoke a range of GT malformations and degrees of hypospadias depending upon when exposure occurs and by what extent urethral morphogenesis is disrupted [10]. By E17.5, the male urethral primordium has divided into a central urethral tube and residual ventral seam. Therefore, for this study we modeled mouse GT development over the critical four-day period of gestation (E13.5-E17.5) that encompasses three major events in GT development: formation of endodermal urethral tube during elongation of the urogenital sinus (E13.5); patterning of the preputial mesenchyme during elevation of the urethral folds (E15.5); and sexually dimorphic changes leading to urethral fusion/septation at the ventral midline in males (E17.5).

We modeled gestational days E13.5 to E17.5 using an idealized two-dimensional (2D) cross-section (with dorso-ventral and medio-lateral axes) that represents GT morphology midway along its proximo-distal axis [10,51,52]. As shown in Fig. 1, the initial rendering (E13.5) of the modeled 2D cross-section consists of an exterior ectodermal jacket, an interior bud-like hillock of mesenchymal cells and an endodermal sinus; the entire structure was surrounded by a fluid medium. Our previous systems toxicology model of male reproductive developmental toxicity [44] identified vascular/angiogeneic processes as one possible target for chemical disruption (albeit not hypospadias). In mice, hypospadias is often accompanied by gross enlargements of the GT vasculature and reductions in HOXA13-dependent expression of EphA6 and EphA7 in the GT vascular endothelia [55]. The current GT model could be thus expanded by incorporating ephrin-signaling and angiogenesis as a future goal.

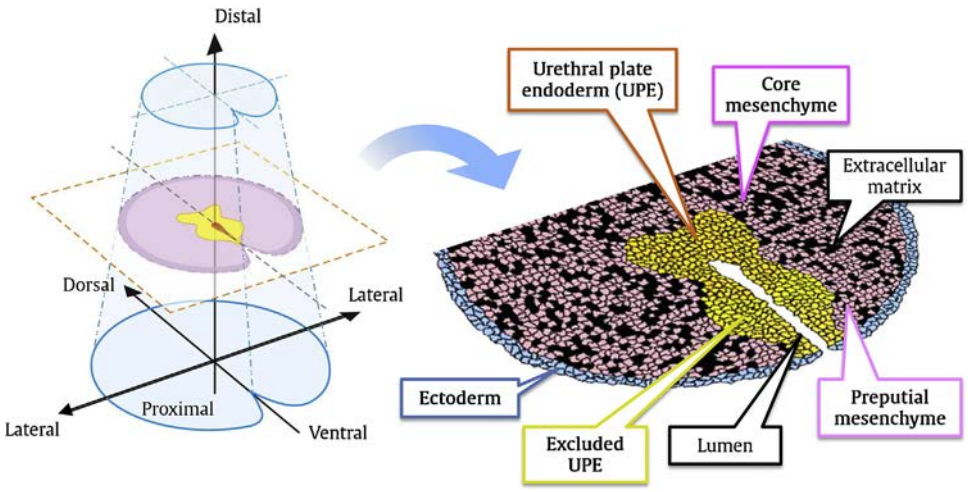

Fig. 1. Cell and tissue geometry in the model of genital tubercle development. (Left) Three-dimensional structure of the early genital tubercle showing dorso-ventral, medio-lateral and proximo-distal axes. (Right) Initial geometry of the modeled two-dimensional cross-section. Cell types as labeled.

2.2. Cellular dynamics

Simulations of GT developmental dynamics were constructed using a multicellular agent-based model in CompuCell3D, Version 3.7.4 (CC3D; http://CompuCell3D.org). This is a cellular Potts model [56,57] in which individual cells are treated as autonomous agents influenced by mechanical forces and chemical signals. The cells interact in a shared physical environment, modeled as a 2D lattice, in which each cell occupies multiple lattice sites. Our targeted cross-section of the GT is approximately 150 biological cells wide at E13.5 [37], but this was quarter-scaled in the modeled to speed simulation time: *i.e.*, ~38 simulated cells (agents) spanning 1000 × 750 lattice sites (pixels). Within this lattice, cells change shape or move by extending into an adjacent pixel or retracting from an occupied one [58]. Although these movements are stochastic, they are governed by a pseudo-energy Hamiltonian (details below) following a Metropolis Monte Carlo approach [59]. Model dynamics were thus discretized in Monte Carlo Steps (MCS)—each MCS corresponding to a sweep of calculations across the entire lattice. The conversion to actual time is approximately 1000 MCS per day of gestation. Each simulation began with a 200-MCS equilibration period and then continued for 4000 MCS to cover both urethral plate maturation during E13.5–E15.5 and urethral fusion/septation during E15.5–E17.5.

As noted above, dynamics in the model were governed by a pseudo-energy Hamiltonian, which had terms for cell incompressibility and cell-cell contact energies. Incompressibility was represented by pseudo-energy terms with a quadratic dependence on how much each cell's area (A_i) differed from its current target area ($A_{i,0}$), *i.e.*, $E_i = \lambda_i (A_i - A_{i,0})^2$, where λ_i denotes stiffness of the i^{th} cell. As cells grew in size, their target areas changed accordingly. Mitosis was implemented as an equal division when the computational cell reached a particular size. If a cell grew above a defined mitosis cut-off area, the cell would then be split into two daughter cells, each having a target are equal to half that of the mother cell. All cells in the model were initialized with $\lambda = 2$, a mitosis cut-off of 134 pixels, and target areas randomly selected from 67 to 133 pixels. This initialization ensured asynchronous cell cycle progression across the tubercle. The contact energy terms then determined how cells segregated. These terms were proportional to the length of each type of cell-cell (or more generally agent-agent) contact with a different proportionality constant defined for each pair of cell/agent types. The matrix of cell/agent contact energies is shown in Table 1. In general, homotypic contact energies were set lower than heterotypic ones to prevent extensive mixing of cell types. Apoptosis was represented by a stochastic fragmentation, as described below.

Table 1
Contact energy matrix for all agent/cell types in the genital tubercle model: Medium; LM, lumen; EC, ectoderm; UPE, urethral plate endoderm; eUPE, excluded urethral plate endoderm; CM, core mesenchyme; PM, preputial mesenchyme; and ECM, extracellular matrix. Smaller values represent more favorable adhesive contacts. The effective temperature (which determines the energy scaling) was 10.

Agent Type	Medium	LM	EC	UPE	eUPE	CM	PM	ECM
Medium	10	10	10	10	10	10	10	10
LM		2	10	10	10	10	10	10
EC			5	10	10	10	10	10
UPE				5	5	10	10	10
eUPE					5	10	10	10
CM						5	5	10
PM							5	10
ECM								10

The GT model prototype included five distinct cell types: ectoderm (EC), urethral plate endoderm (UPE), excluded UPE (eUPE), core mesenchyme (CM), and preputial mesenchyme (PM). The specifics are defined below. The model also had 'agents' representing the mesenchymal extracellular matrix (ECM), the lumen (LM) of the prospective urethral tube, and the surrounding amniotic fluid (Medium). Epithelial ectoderm and endoderm tissues (EC, UPE, and eUPE) in the model were made stiffer than mesenchyme by including elastic pseudo-energy terms for connections between adjacent cells, so called focal point plasticity [60,61].

2.3. Signaling network

The GT development model includes a minimal signaling network with cell-type-specific responses to three key molecular signals—SHH, FGF10, and androgen (Fig. 2). Note that in this initial prototype, the ectoderm plays no role in the minimal signaling network; however, ectoderm may play a key role in GT organization [32,35], but we focus here on endodermal-mesenchymal interactions mediated by SHH and FGF10, which are in turn modulated by androgen. SHH and FGF10 are the most well studied morphogen gradients in GT development. SHH is secreted by endoderm cells and induces mesenchymal growth and FGF10 secretion—acting through PTCH1, SMO, GLI1, GLI2, and GLI3 [16,37,49,62]. The FGF10 secreted by mesenchymal cells acts through FGFR2IIIb to induce endodermal growth and regulate epithelial stratification in endo- and ectoderm [32,35]. These reciprocal actions form the central

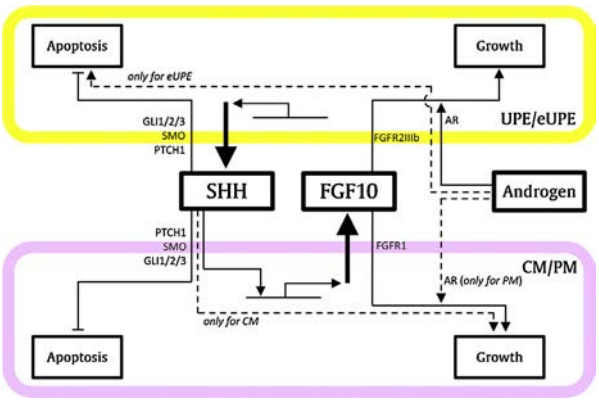

Fig. 2. Signaling network in the genital tubercle development model. This minimal signaling network coordinates three primary pathways (SHH, FGF10, and androgen) and was constructed based on previous experimental studies listed in Supplementary material S2. Boxes represent signaling molecules and linked behaviors that are explicitly included in the model. Intermediate molecules in the relevant pathways are noted along the connecting arrows. The two thickest arrows represent secretion of SHH and FGF10. The arrows with dashed lines represent links that are present in only one type of endodermal or mesenchymal cell (as noted along each dashed line).

SHH-FGF10 positive feedback loop driving GT outgrowth. During male sexual differentiation, androgen signals modulate this positive feedback through androgen responsive signaling (androgen receptor, AR) by inducing further expression of FGFR2IIIb (which has an upstream AR responsive element) and thus increase the UPE's response to FGF10 signals [16].

Several assumptions were made in the initial prototype model to address additional controls of cell growth. First, experiments suggest that the AR pathway promotes mesenchymal proliferation [10,18] although the mechanism is unclear. Thus, we added a link from FGF10 to mesenchymal growth; our hypothesis was that androgen signals induce increased expression of FGFR1, a receptor that binds FGF10 in the GT mesenchyme [62,63]. This connection leads to androgen-responsive growth of mesenchyme that parallels that of the urethral endoderm. Second, *in vivo* histology reveals differential growth of core and preputial mesenchyme from E15.5 to E17.5 [51,52]. To recapitulate this differential growth in the GT model, we limited androgen-driven FGF10-responsiveness to preputial mesenchyme (PM) in the lateral aspects of the GT and added a link between SHH and growth of core mesenchyme (CM) more centrally located in the model. Although these are hypothetical (implicit) connections, we state them explicitly as assumptions to yield correct emergent tissue behaviors.

Spatially and temporally varying concentrations of SHH and FGF10 were specified in the model as secreted diffusible chemicals. All endodermal cells were assumed to secrete SHH at a constant rate, which is consistent with patterns of *Shh* gene expression during these stages [41,42]. Each CM and PM cell secreted FGF10 in response to SHH according to a saturable sigmoidal function

$$V = V_{max} \times \frac{[SHH]}{EC_{50} + [SHH]},$$

where V is a cell's rate of FGF10 secretion, V_{max} is its maximum rate, $[SHH]$ is the local SHH concentration, and EC_{50} is the SHH concentration yielding a half-maximal effect. The model parameters used in this equation are listed in the "Secretion of FGF10" entries in Table 2. Note that chemical concentrations were recorded in arbitrary concentration units (cu), but were only important in terms of ratios to the matching EC_{50} values. Within cells of the GT, the diffusion constant of SHH was set to one-eighth that of FGF10 (0.5 *versus* 4.0 pixels^2/MCS), reflecting the rate difference between transcytosis (SHH) and simple diffusion (FGF10) [64]. To appropriately limit the range of these diffusible signals, decay constants for both SHH and FGF10 were set to 1.0×10^{-3} per MCS. To represent loss of any SHH or FGF10 that diffused into the surrounding amniotic fluid, the decay constants in the surrounding amniotic fluid (*e.g.*, Medium) were set to 1000 per MCS.

Table 2 also includes parameters that determine how SHH and FGF10 drive cell growth. The rate at which a particular cell grows is an additive combination of its basal growth rate (0.02 pixels/MCS for all cell types) and the rate(s) induced by SHH and/or FGF10. These induced rates follow a saturable sigmoidal function, similar to that given above, such that

$$R = R_{basal} + R_{max,FGF10} \times \frac{[FGF10]}{EC_{50,FGF10} + [FGF10]} + R_{max,SHH} \times \frac{[SHH]}{EC_{50,SHH} + [SHH]},$$

where R is a cell's growth rate and each signal has an independent maximal effect (R_{max}) and concentration at which its effect is half-maximal (EC_{50}). If a cell type's growth rate does not depend on SHH, then its $R_{max,SHH}$ is zero (and is not listed in Table 2). The model treated the effects of androgen signaling on FGF10-responsive growth rates as a switch between androgen-negative and androgen-positive parameter values (An- and An+ in Table 2). In the presence or absence of androgen signals, $R_{max,FGF10}$ was three-fold higher in PM than UPE or eUPE. This difference in growth rates was needed to ensure faster growth of bulk mesenchyme (which needs to grow as the square of the GT radius, r^2) compared to surface epithelium (which only needs to grow linearly with r).

2.4. Programmed cell death

Cells in the model stochastically committed to programmed cell death according to a cell-specific apoptosis probability. The basal probability for mesenchyme and endoderm cells (CM, PM, UPE, and eUPE) was 1.0×10^{-5} per MCS. This probability was then reduced via a sigmoidal function to model SHH inhibition of apoptosis [38,49]

$$P = P_{basal} - P_{max,SHH} \times \frac{[SHH]}{EC_{50,SHH} + [SHH]},$$

where P is a cell's apoptosis probability, P_{basal} is the basal probability, and $P_{max,SHH}$ is the maximum amount by which SHH could reduce the probability. As shown in Table 1, $P_{max,SHH}$ was always chosen to be less than P_{basal} to make sure the total probability never went below zero. Apoptosis in the UPE is also promoted by androgen signals through TNFα [18]. This effect was included by switching P_{basal} and $P_{max,SHH}$ to 100-fold higher values for UPE cells when androgen signaling was active. These parameters resulted in 2–4% of the cells undergoing a basal rate of apoptosis over the course of the simulation. We do not make an assumption that this basal apoptotic rate is biologically relevant for GT development—it was introduced primarily to enhance biological variability across multiple GT simulations.

2.5. Androgenization

Sexual dimorphism from E15.5 to E17.5 (2000–4000 MCS) that follows from androgen signaling was implemented in the model as the previously noted switching of parameters from androgen-negative (An-) to androgen-positive (An+) values. Since the model does not simulate vascular perfusion, we assumed that dispersal of blood-borne hormonal signals was rapid and uniform across different embryonic tissues [38,65]. Thus, we implemented the switch to androgen-positive parameter values simultaneously for all cells at E15.5 (2000 MCS). This corresponds to the anticipated onset of

Table 2
Cell behaviors and control signals represented in the multicellular agent-based model of genital tubercle development. Growth rates reported in pixels/MCS, secretion rates in cu/cell/MCS, and apoptosis as a probability per cell per MCS. Each EC_{50} is reported in cu. Androgen-negative and androgen-positive parameter values are indicated as An- and An+.

Cell Type	Behavior	Control Direction	Signal	Max Effect An-; An+	EC_{50} An-; An+
Ectoderm (EC)	Growth	Basal	–	0.02	–
Urethral Plate Endoderm (UPE)	Growth	Basal		0.02	200; 50
		Activated by	FGF10[a,b]	0.03; 0.12	
	Secretion of SHH	Basal	–	0.1	–
	Apoptosis	Basal		1×10^{-5}	–
		Inhibited by	SHH[c]	5×10^{-6}	40
excluded Urethral Plate Endoderm (eUPE)	Growth	Basal		0.02	200; 50
		Activated by	FGF10[a,b]	0.03; 0.12	
	Secretion of SHH	Basal	–	0.1	
	Apoptosis	Basal		1×10^{-5}; 1×10^{-3}	–
		Inhibited by	SHH[a,c]	5×10^{-6}; 5×10^{-4}	40; 40
Core Mesenchyme (CM)	Growth	Basal		0.02	–
		Activated by	SHH[d]	0.05	40
		Activated by	FGF10[d]	0.05	200
	Secretion of FGF10	Activated by	SHH[e]	20	40
	Apoptosis	Basal		1×10^{-5}	–
		Inhibited by	SHH[c]	5×10^{-6}	40
Preputial Mesenchyme (PM)	Growth	Basal		0.02	
		Activated by	FGF10[b,d]	0.1; 0.4	200; 50
	Secretion of FGF10	Activated by	SHH[e]	20	40
	Apoptosis	Basal		1×10^{-5}	–
		Inhibited by	SHH[c]	5×10^{-6}	40

[a] [16].
[b] [18].
[c] [80].
[d] [11,79].
[e] [49].

fetal Leydig cell function [66]. Delayed or reduced androgen levels, defined here as 'androgen insufficiency', was modeled by a linear reduction in the androgen-positive growth and apoptosis rates. For example, 67% androgen sufficiency reduced the maximal androgen-positive FGF10-driven growth rate of endoderm from 0.12 pixels/MCS to 0.09 pixels/MCS (*i.e.*, $0.03 + 0.67(0.12 - 0.03)$). For interpreting the simulated phenotypes, 'urethral fusion' was defined as the moment when initially separate endoderm layers made contact and adhered to one another at the ventral midline and 'urethral septation' was defined as the post-fusion separation and exclusion of eUPE from definitive urethral endoderm by invading ventral mesenchyme.

2.6. Modeling software and computing platform

The model was scripted in XML and Python, Version 2.7 (http://python.org) using the CompuCell3D integrated development environment (IDE), Twedit++. The python code for running the simulation in CompuCell3D v2.7 is provided as Supplementary material S1 (see Supplementary material S1 in the online version at DOI: 10.1016/j.reprotox.2016.05.005). The initial cell configuration was rendered in a *.piff file using CellDraw (http://www.compucell3d.org/). Individual simulations (n = 10 for each parameter set) ran on a Mac Pro computer with dual 2.93 GHz 6-Core Intel Xeon processors and 32 GB 1333 Mhz DDR3 ECC memory. For sensitivity analysis, batch simulations (n = 4) ran on a 1400-CPU Linux cluster at EPA's National Computer Center using a combination of parallel methods, including workload management, software image rendering, and R statistics post-processing (Version 3.1.1) [67].

3. Results

3.1. Sex-Specific genital tubercle development

Model outputs corresponding to mouse gestation days E13.5 to E17.5 are shown in Fig. 3 and Supplemental materials S2 and S3 (see Supplementary materials S2 and S3 in the online version at DOI: 10.1016/j.reprotox.2016.05.005) (1 day = 1000 MCS). GT development for modeled male and female embryos is the same up to E15.5 (2000 MCS), but diverges thereafter. Pre-and post-divergence growth of the endoderm and mesenchyme was driven by SHH-FGF10 signaling. Both SHH and FGF10 concentrations rose throughout the simulation; however, due to differences in diffusion kinetics SHH signals remained in close proximity to the endoderm whereas the FGF10 gradient reached laterally into the mesenchyme (Fig. 3). Before sexual differentiation, the combined effects of SHH and FGF10 signaling increased the number of cells of all modeled cell types (Fig. 4).

Androgen was introduced to the simulation by switching parameters in the male simulation at E15.5 (2000 MCS). This demonstrated that urethral tube closure is an emergent property of the simulation that is also sex-specific. After the switch to higher androgen-positive responsiveness to FGF10 signals, mesenchymal growth in the male simulation accelerated strongly (Fig. 4). By E17.5, the number of PM cells in the male simulation was approximately double the number of PM cells in the female simulation (n = 10). The increased number of PM cells led to condensation (*i.e.*, increased cell density) in the ventral mesenchyme and forced the physical fusion and septation of the male urethral tube, which roughly recapitulates the anatomical features of urethral fusion in the rodent [10,51,52]. Urethral fusion and septation created a multi-layered endoderm that bordered, closed off and internalized the prospective urethral lumen. In the feminized simulation, cells continued to grow in response to FGF10 signaling, but at lower

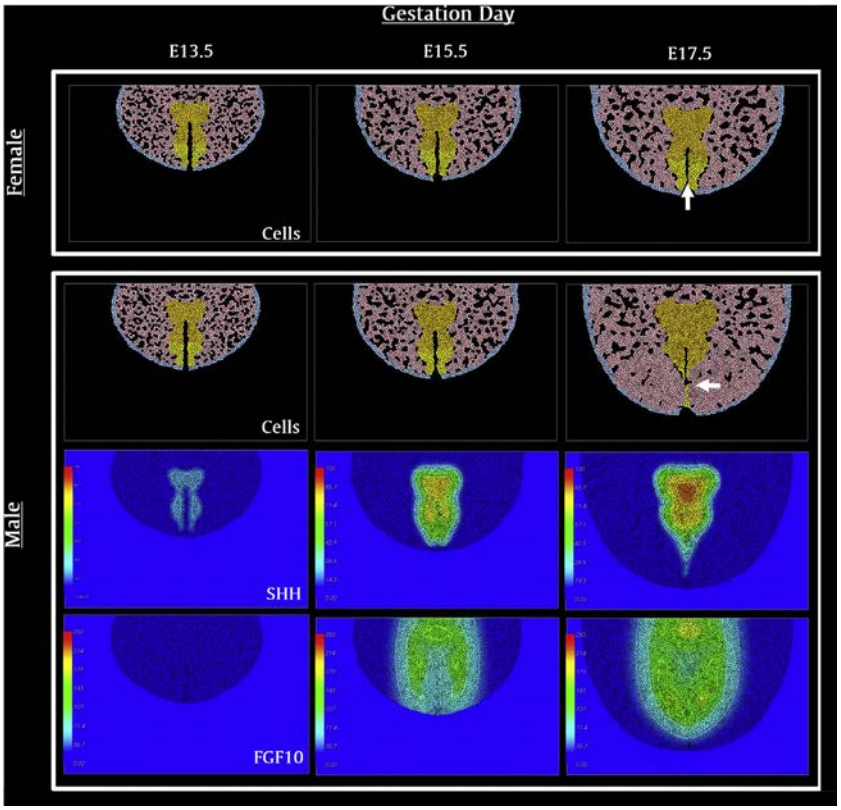

Fig. 3. CompuCell 3D model replicating sexual dimorphism in genital tubercle development. Male and female simulations show identical growth from E13.5 to E15.5. Androgen signaling in the male lead to accelerated mesenchymal growth and urethral tube apoptosis from E15.5 to E17.5, resulting in fusion and septation of the urethral plates (white arrow). The female urethral lumen remained open to the amniotic fluid medium at E17.5.

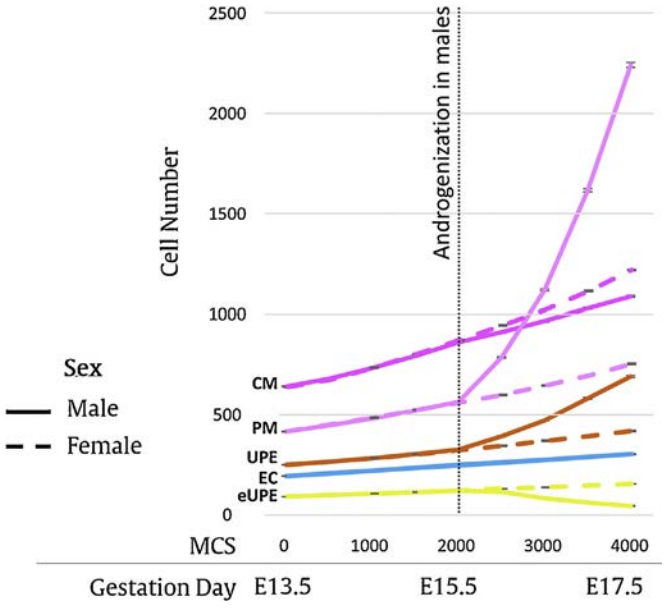

Fig. 4. Male and female cell growth in the model of genital tubercle development (n = 10). Androgenization in males begins at 2000 Monte Carlo Step. Male and female simulations are indicated with solid and dotted lines respectively. Cell types are indicated on each curve.

androgen-negative rates; without condensation/fusion/septation, the female urethral opening remained open to the amniotic fluid throughout the simulation.

The ventral urethral tube in male simulations also displayed strong increases in apoptosis from E15.5 to E17.5. The degree of endodermal apoptosis was specified in the model via the androgen-positive apoptosis probabilities. These had to be large for proper urethral tube closure—a result that supports the observation of Baskin et al. [36] and Chen et al. [18] that AR modulates urethral tube closure through endodermal apoptosis; as well as the observation of Griffith and Hay [68], Mori et al. [69], and Sun et al. [70] that epithelial apoptosis plays a similar role in palate fusion. Genital tubercle development is in some ways similar to other developmental processes leading to fusion events and closures [71]; there are, however, nuances on the cellular logistics of how fusion events are regulated and implemented in different embryonic structures. For instance, the current simulation did not support the hypothesis that epithelial-mesenchymal transition played a role in urethral tube closure [32,36].

3.2. Effects of SHH insufficiency

Varying degrees of SHH insufficiency were modeled functionally, *i.e.*, by reducing the maximal rate of SHH secretion. This functional approach simulates hypothetical genetic and/or environmental perturbations of SHH secretion, including genetic polymorphisms that may impact the regulation of SHH synthesis, or cholesterol deficiency that may impair SHH esterification, or maternal alcohol consumption that may phenocopy the loss of Shh genetic function [25,72,73]. As shown in Fig. 5A, reducing SHH sufficiency resulted in non-linear decreases in all mesenchymal and endodermal cell populations (CM, PM, UPE, and eUPE; n = 10). Some of the decreases were directly linked to SHH insufficiency through increased apoptosis (and reduced growth in CM), but most were indirectly linked through reduced SHH-dependent FGF10 secretion (Fig. 2).

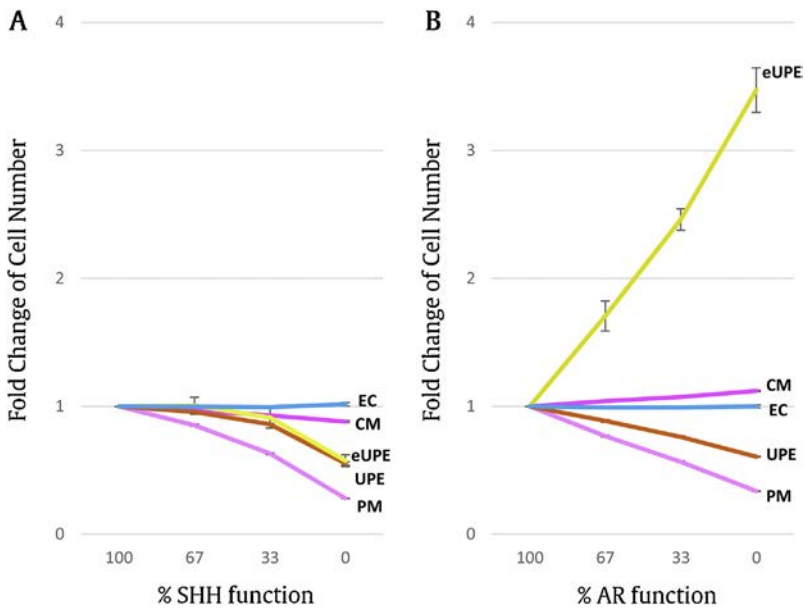

Fig. 5. Fold change of cell number with different levels of SHH and AR function in the model of genital tubercle development (n = 10). Fold changes are relative to 100% AR and 100% SHH function.

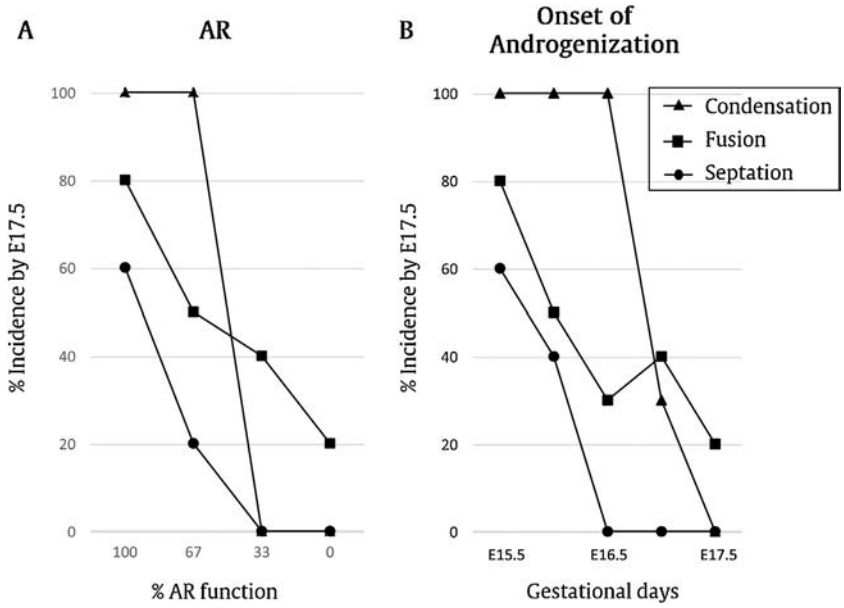

Fig. 6. Effects of AR sufficiency and androgenization delay on emergent features of urethral tube closure (n = 10). (A) The incidence of three emergent features (condensation of ventral mesenchyme, fusion of urethral folds, and septation of the urethral endoderm) decreased as AR sufficiency decreased. Simple averaging the incidence of the three features resulted a 'closure index' that dropped monotonically from 0.80 for the masculinized condition (100% AR sufficiency) to 0.57 (67% AR sufficiency), 0.13 (33% AR sufficiency), and finally 0.07 for the feminized condition (0% AR sufficiency). (B) The emergent features were also readily disrupted by delayed androgenization (normally occurring at E15.5).

3.3. *Effects of AR insufficiency*

Recent attention has been devoted to defining how much reduction in fetal testosterone production was required to invoke adverse effects on male reproductive tract development in rats exposed *in utero* to phthalates [74,75]. Androgen-sensitive development of the GT model was tested by varying the amount and timing of AR activation. Varying degrees of AR insufficiency were modeled with a functional approach that reduced the maximal androgen-positive effects of AR-linked behaviors (growth response to FGF10 in UPE, eUPE and PM; apoptosis rates in eUPE). A 'male' simulation with no androgen (*e.g.*, 0% AR sufficiency) was feminized with respect to urethral fusion and septation. The feminized model is not precisely a simulation of the 'female' GT phenotype, because the simulation does not yet include estrogen-responsive pathways, which play important roles during GT development during the neonatal period [3]. The model can, however, be used to test how incremental changes in androgenization would be predictive of androgen-sensitive GT development. This was accomplished by running the model at 33% and 67% androgen sufficiency and comparing the results to 0% (*e.g.*, feminized) and 100% (*e.g.*, masculinized) conditions. Incrementally decreased levels of AR sufficiency resulted in progressively fewer PM and UPE cells, and more CM and eUPE cells over the same time course (Fig. 5B). These

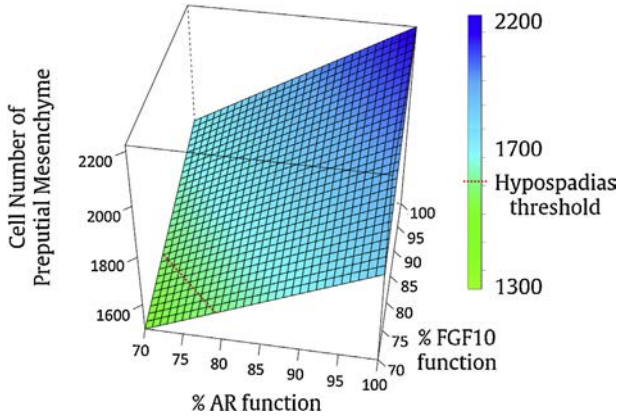

Fig. 7. Sensitivity analysis of combined FGF10 and AR insufficiency. A total of 64 simulations were run with FGF10 and AR function varying independently from 70 to 100% sufficiency (all at 100% SHH function; four replicates for each combination). Each location on the interpolated surface could be viewed as a simulated individual, with the given average cell number achieved for that individual's specific combination of FGF10 and AR functional sufficiency. The dashed line separates combinations of FGF10 and AR function for which the number of preputial mesenchyme cells was above or below the model's inferred hypospadias cut-off.

effects on PM and UPE cell numbers follow from a reduction in their normal androgen-positive growth rates whereas effects on the eUPE resulted from reduced androgen-positive apoptosis. The small effect on CM cells was a secondary result of reduced PM cell number, which allowed CM cells to remain closer to the UPE and thus be more strongly affected by SHH elaborated from the UPE. These outcomes phenocopied the region-specific effects of androgen signaling on both endodermal and mesenchymal growth in the GT during sexual differentiation [10].

For any single level of AR sufficiency, replicate simulations (n = 10) had less than 2% variation in cell numbers. Nonetheless, the simulations' stochastic nature resulted in probabilistic outcomes that could be assessed on three emergent features underlying urethral tube closure: condensation, fusion, and septation (Fig. 6). At 100% AR sufficiency, all male simulation replicates resulted in condensation of the ventral mesenchyme, recapitulating the *in vivo* observation [51,52]. Only 8 of 10 runs completed fusion and 6 of 10 completed septation during the course of the simulation. Simple averaging these three features resulted a 'closure index' of 0.80 for 100% AR sufficiency. Reducing AR sufficiency decreased the incidence of all three features, and therefore the closure index, in the simulation runs (Fig. 6A). The closure index dropped monotonically from 0.80 for the masculinized condition (100% AR sufficiency) to 0.57 (67% AR sufficiency), 0.13 (33% AR sufficiency), and finally 0.07 for the feminized condition (0% AR sufficiency). The incidences of condensation, fusion, and septation were also reduced if androgenization was delayed from the critical time of introduction to the GT model at 2000 MCS (E15.5; Fig. 6B). A one-day delay had no effect on mesenchymal condensation but lowered the incidence rate of successful fusion by half and led to a failure of septation in all replicates. Complete urethral tube closure required the PM population to achieve a quorum in numbers during the E15.5-E17.5 window.

3.4. Combined insufficiencies of SHH, FGF10, and AR

To examine how chemical perturbation of AR activity interacts with genetic deficiency of SHH and/or FGF10 signaling, we ran male GT model simulations at either 70% or 100% SHH sufficiency and 70–100% sufficiency of FGF10 and AR function (128 total simulations with 4 replicates for each parameter set). Fig. 7 plots the number of PM cells observed at E17.5 (4000 MCS). As a useful threshold reference, the number of PM cells observed at E17.5 with a 0.5-day delay of androgenization was approximately 1600–a level that yielded a 50% incidence of endodermal fusion. At full-strength SHH function the final PM population exceeded this threshold value for all simulations having AR and FGF10 above 80% sufficiency (Fig. 7). In comparison, reducing SHH function to 70% pushed the PM population below threshold for either 70% FGF10-/95% AR-sufficiency or 95% FGF10-/70% AR-sufficiency (data not shown). This is the first *in silico* evidence to show how genetic deficiencies can increase hypospadias risk with prenatal environmental exposures.

4. Discussion

Computer simulations that predictively model sexual dimorphism of the GT provide a useful resource to translate chemical-target bipartite networks and their developmental consequences across the human-relevant chemical universe. The 'virtual tissue' prototype constructed here for the GT modeled several morphoregulatory signals underlying differential growth and sexual dimorphic patterning, including SHH, FGF10, and androgen. The signals invoked local changes in cellular behaviors such as differential adhesion, cell motility, proliferation, and apoptosis and collectively enabled GT growth, urethral tube closure and internalization as emergent features realized in an androgen-dependent manner. Simulating a complex embryological system in this manner has potential applications for high-throughput hypothesis-based testing and translating chemical-biological interactions into tissue-level predictions.

The virtual GT model identified androgen-dependent mesenchymal proliferation and endodermal apoptosis as two key events in urethral tube closure. This recapitulates the *in vivo* biology of rodent GT development [36,51,52]. Although the present cross-sectional (2D) spatial model had discriminatory potential for sexual dimorphism of urethral closure, it missed aspects of male urethrogenesis requiring the third dimension. Proximo-distal cell migration and ECM expansion, for example, is not represented in the current model. Histologically, the *in silico* model showed less pronounced ECM in the ventral fusion zone than expected from the *in vivo* studies, although the localized proliferation created a high cell density region at the nascent site of septation that is consistent with *in vivo* findings [11,52]. We did not consider a role for biomechanical forces in this study, although mechanical compression of mesenchyme is a differentiation factor in other systems [76] and could be important here as well. As such, future improvement in the virtual GT model should strive toward a more realistic representation of the ECM and mechanical forces in 3D.

Apoptosis in the urethral epithelium of the virtual GT model recapitulated at least some aspects of the *in vivo* biology of urethral fusion and septation [3,18,35,36,38,50]. Recent studies of mouse urethral closure, for example, demonstrated the necessity of epithelial apoptosis at the ectoderm-endoderm junction to permit androgen-dependent separation of urethral epithelium from dermal (foreskin) ectoderm [3]. The virtual GT model recapitulated the essential role of SHH- and androgen-dependent endodermal cell death in urethral fusion and internalization for male embryos; however, it did not faithfully recapitulate the residual apoptosis observed in female embryos [3]. Therefore, future improvement in the virtual GT model should strive toward a more realistic representation of programmed cell death patterns during sexual dimorphism.

The virtual GT model predicts a key role for the differential androgenized growth response of preputial (PM) *versus* core (CM) mesenchyme, consistent with the cellular localization of AR *in vivo* [3,16,17]. This effect was mediated by androgen-dependent FGF10 signaling. FGFR1, a receptor that binds FGF10 in the GT mes-

enchyme [62,77], has no identified ARE (AR-responsive element) in its promoter region [78]; however, the critical receptor mediating FGF10 signaling is FGFR2 [16]. This involves a reciprocal loop with SHH that acts to sustain endodermal proliferation [11,49]. Although SHH up-regulates FGF10, *Shh* expression is not thought to be a downstream target of the androgen pathway; however, expression of *Fgfr2iiib* (the epithelial isoform of *Fgfr2*) is up-regulated by AR activation [79]. The virtual GT model's capacity to reproduce male GT development from E13.5-E17.5 in a manner that involved regulation by SHH-FGF10 signals and AR-FGFR2 pathways was thus consistent with the known embryology. On the other hand, recent studies demonstrated the importance of endoderm-specific deletion of *Fgfr2iiib* results in mild hypospadias due to incomplete septation and internalization of the urethra, whereas ectodermal deletion causes severe hypospadias due to failure of urethral fusion and internalization [32]. So although FGFR2 is a direct link between hormonal and genetic regulation of external genital development [10,37,38], urethral tubulogenesis and sexually dimorphic patterning are controlled by discrete regions of FGFR2 activity. Implementation of discrete regions of *Fgfr2iiib* activity in the GT model remains for future development.

The current GT model was able to simulate a virtual population of individuals each incurring multiple low-level disturbances across SHH, FGF10, and AR pathways. This virtual epidemiology simulation demonstrated how the link between hormonal and genetic regulation of external genital development could be translated to the population level for assessing susceptibility to endocrine disrupting chemicals. Hypospadias in humans has been clearly associated with genetic variants in SHH and FGF10 [25], but there is limited evidence associating hypospadias with endocrine disrupting compounds [1,31]. Prenatal exposure to environmental chemicals such as bisphenol A, flutamide, phthalates, and vinclozolin may disrupt fetal androgen-responsive pathways in animal models [27,28,36], and studies with phthalate exposure in pregnant rats have begun to define how much reduction in fetal testosterone production was required to invoke adverse effects on male reproductive tract development [74,75].

Virtual disruption of urethral closure in the GT simulation generated a monotonic dose response with the effects observable at the lowest drop in AR sufficiency tested here (33% reduction). This *in silico* prediction is consistent with *in vivo* 'biologically relevant reduction' (BRR) in fetal testosterone invoking elements of the rat phthalate syndrome [74,75]. The BRR derives from logistic regression models of some but not all male reproductive outcomes. For example, reproductive tract malformations were observed in 17% of male rats prenatally-exposed to a phthalate mixture (GD8-PND3) when fetal testosterone was reduced by about 25% [74], or to dipentyl phthalate (GD14-18) when fetal testosterone production was reduced by >45% [75]. A caveat, however, is that hypospadias was "difficult to model" *in vivo* due it being a generally high-dose phenomenon and a "very subtle effect that can be easily overlooked during necropsy". Dynamical simulations with the virtual GT model indicate that circumstances underlying hypospadias are consistent with BRRs <33% range. Furthermore, factors other than androgenization may contribute to developmental defects of the GT. Virtual disruption of urethral closure in the GT simulation showed how a minor disruption of AR signaling could be well tolerated by most exposed fetuses, but lead to hypospadias in susceptible populations with subnormal SHH and/or FGF10 function. Further investigation is needed to understand (1) the spatio-temporal dynamics of fetal testosterone reductions over the course of GT development; and (2) how specific SHH and FGF10 variants or pathway-level disruptions might affect SHH and FGF10 signaling and contribute to differential endocrine-disruptor susceptibility in human populations.

The present model is a minimal representation of mouse GT development. A number of additional features could expand its scope and comprehensiveness. Since the model considers only a 2D cross-section of the GT, it does not capture the proximo-distal cell movements that at least partly cause internalization of the urethral tube in males [10]. In addition, the model captures endodermal cell growth, but not stratification—*i.e.*, it omits the endoderm's functionally important development of epithelial structure [32]. The model marginally captures this stratification though the contact energy matrix and elastic links between UPE cells but future models could make epithelial polarization much more explicit. The model should be extended to include the ectoderm's FGF10 signaling and stratification, which are thought to play important roles in urethral tube closure [32,35], and as well incorporate addition nodes such as signaling through Wnt, retinoid, estrogen and ephrinB pathways as well as vascular tissue. The model should also be expanded to incorporate the estrogenic pathway that is necessary for female GT development [3] and that may contribute to the risk for hypospadias [45]. Finally, it must be emphasized that lower urinary and reproductive system development in mouse and human are not equivalent [7]. Terms have been drawn from human anatomy to incorrectly describe similar, but distinct structures between rodent-humans and the common diagnosis of hypospadias as applied to ventral defects of the GT, where diagnosing hypospadias based only on analysis of gross morphology and transverse sections of embryonic GTs should be confirmed at juvenile stages or older [6].

In conclusion, this study demonstrates a proof-of-concept *in silico* multicellular modeling and simulation approach to generate and evaluate new research hypotheses and conduct virtual epidemiology of gene/environment interactions for a multifactorial adverse developmental outcome potentially linked to endocrine disruption. Chemical exposures may disrupt male reproductive development through molecular targets other than AR, such as cytochrome P450s, G-protein-coupled receptors, vascularization remodeling proteins, and the retinoic acid signaling pathways [44]. Eventually the model can be expanded to capture these molecular targets in explorations of adverse outcome pathways on male reproductive tract defects. This would facilitate incorporation of *in vitro* profiling data from high-throughput screens such as ToxCast, to knowledge-driven tissue architectures to predict adverse outcomes, thereby providing an *in silico* platform for probabilistic prediction of hypospadias risk across combinations of minor perturbations to the GT system at various stages of embryonic development.

Conflict of interest

The authors declare they have no actual or potential competing financial interests.

Disclaimer

The views expressed in this article are those of the authors and do not necessarily reflect the views or policies of the U.S. Environmental Protection Agency. Mention of trade names or commercial products does not constitute endorsement or recommendation for use.

Acknowledgements

We thank Muhammad Ahsan, Dustin Kapraun, and Caroline Ring for technical advice; and Woodrow Setzer and Nisha Sipes for helpful comments on the manuscript. This research was funded by the U.S. EPA Chemical Safety for Sustainability research Program. M.S.H. was supported in part by U.S. EPA Science to Achieve Results (STAR) Program (#83573601) under a cooperative agreement.

References

[1] S.L. Carmichael, G.M. Shaw, E.J. Lammer, Environmental and genetic contributors to hypospadias: a review of the epidemiologic evidence: birth Defects Res, A Clin. Mol. Teratol. 94 (2012) 499–510.
[2] L.F. van der Zanden, I.A. van Rooij, W.F. Feitz, B. Franke, N.V. Knoers, N. Roeleveld, Aetiology of hypospadias: a systematic review of genes and environment, Hum. Reprod. Update. 18 (2012) 260–283.
[3] Zheng, Z., Armfield, B.A., and Cohn, M.J. (2015) Timing of androgen receptor distribution and estrogen exposure underlies a spectrum of congenital penile anomalies. 10.1073/pnas.1515981112.
[4] L.J. Paulozzi, J.D. Erickson, R.J. Jackson, Hypospadias trends in two US surveillance systems, Pediatrics 100 (1997) 831–834.
[5] C.P. Nelson, J.M. Park, J. Wan, D.A. Bloom, R.L. Dunn, J.T. Wei, The increasing incidence of congenital penile anomalies in the United States, J. Urol. 174 (2005) 1573–1576.
[6] B.J. Schlomer, M. Feretti, E. Rodriguez Jr., S. Blaschko, G. Cunha, L. Baskin, Sexual differentiation in the male and female mouse from days 0 to 21: a detailed and novel morphometric description, J. Urol. 190 (2013) 1610–1617.
[7] K.M. Georgas, J. Armstrong, J.R. Keast, C.E. Larkins, K.M. McHugh, E.M. Southard-Smith, M.J. Cohn, E. Batourina, H. Dan, K. Schneider, D.P. Buehler, C.B. Wiese, J. Brennan, J.A. Davies, S.D. Harding, R.A. Baldock, M.H. Little, C.M. Vezina, C. Mendelsohn, An illustrated anatomical ontology of the developing mouse lower urogenital tract, Development 142 (2015) 1893–1908.
[8] C. Dravis, N. Yokoyama, M.J. Chumley, C.A. Cowan, R.E. Silvany, J. Shay, L.A. Baker, M. Henkemeyer, Bidirectional signaling mediated by ephrin-B2 and EphB2 controls urorectal development, Dev. Biol. 271 (2004) 272–290.
[9] C. Dravis, M. Henkemeyer, Ephrin-B reverse signaling controls septation events at the embryonic midline through separate tyrosine phosphorylation-independent signaling avenues, Dev. Biol. 355 (2011) 138–151.
[10] A.W. Seifert, B.D. Harfe, M.J. Cohn, Cell lineage analysis demonstrates an endodermal origin of the distal urethra and perineum, Dev. Biol. 318 (2008) 143–152.
[11] A.W. Seifert, C.M. Bouldin, K.S. Choi, B.D. Harfe, M.J. Cohn, Multiphasic and tissue-specific roles of sonic hedgehog in cloacal septation and external genitalia development, Development 136 (2009) 3949–3957.
[12] A.W. Seifert, T. Yamaguchi, M.J. Cohn, Functional and phylogenetic analysis shows that Fgf8 is a marker of genital induction in mammals but is not required for external genital development, Development 136 (2009) 2643–2651.
[13] S. Miyagawa, Y. Satoh, R. Haraguchi, K. Suzuki, T. Iguchi, M.M. Taketo, N. Nakagata, T. Matsumoto, K. Takeyama, S. Kato, G. Yamada, Genetic interactions of the androgen and Wnt/beta-catenin pathways for the masculinization of external genitalia, Mol. Endocrinol. 23 (2009) 871–880.
[14] L. Liu, K. Suzuki, N. Nakagata, K. Mihara, D. Matsumaru, Y. Ogino, K. Yashiro, H. Hamada, Z. Liu, S.M. Evans, C. Mendelsohn, G. Yamada, Retinoic acid signaling regulates sonic hedgehog and bone morphogenetic protein signalings during genital tubercle development, Birth Defects Res. B Dev. Reprod. Toxicol. 95 (2012) 79–88.
[15] A.R. Mazahery, K. Suzuki, A. Nagafuchi, M. Miyajima, N. Nakagata, G.D. Orvis, R.R. Behringer, G. Yamada, Functional analysis of ectodermal β-catenin during external genitalia formation, Congenit. Anom. (Kyoto) 53 (2013) 34–41.
[16] A. Petiot, C.L. Perriton, C. Dickson, M.J. Cohn, Development of the mammalian urethra is controlled by Fgfr2-IIIb, Development 132 (2005) 2441–2450.
[17] K. Agras, E. Willingham, B. Liu, L.S. Baskin, Ontogeny of androgen receptor and disruption of its mRNA expression by exogenous estrogens during morphogenesis of the genital tubercle, J. Urol. 176 (2006) 1883–1888.
[18] H. Chen, W. Yong, T.D. Hinds Jr., Z. Yang, Y. Zhou, E.R. Sanchez, W. Shou, Fkbp52 regulates androgen receptor transactivation activity and male urethra morphogenesis, J. Biol. Chem. 285 (2010) 27776–27784.
[19] S.D. Blaschko, P. Mahawong, M. Ferretti, T.J. Cunha, A. Sinclair, H. Wang, B.J. Schlomer, G. Risbridger, L.S. Baskin, G.R. Cunha, Analysis of the effect of estrogen/androgen perturbation on penile development in transgenic and diethylstilbestrol-treated mice, Anat. Rec. (Hoboken) 296 (2013) 1127–1141.
[20] G. Delbès, C. Levacher, C. Pairault, C. Racine, C. Duquenne, A. Krust, R. Habert, Estrogen receptor beta-mediated inhibition of male germ cell line development in mice by endogenous estrogens during perinatal life, Endocrinology 145 (2004) 3395–3403.
[21] T.F. Lucas, C. Royer, E.R. Siu, M.F. Lazari, C.S. Porto, Expression and signaling of G protein-coupled estrogen receptor 1 (GPER) in rat Sertoli cells, Biol. Reprod. 83 (2010) 307–317.
[22] J.H. Yang, J. Menshenina, G.R. Cunha, N. Place, L.S. Baskin, Morphology of mouse external genitalia: implications for a role of estrogen in sexual dimorphism of the mouse genital tubercle, J. Urol. 184 (2010) 1604–1609.
[23] E. Rodriguez Jr., D.A. Weiss, M. Ferretti, H. Wang, J. Menshenia, G. Risbridger, D. Handelsman, G. Cunha, L. Baskin, Specific morphogenetic events in mouse external genitalia sex differentiation are responsive/dependent upon androgens and/or estrogens, Differentiation 84 (2012) 269–279.
[24] A. Beleza-Meireles, F. Lundberg, K. Lagerstedt, X. Zhou, D. Omrani, L. Frisén, A. Nordenskjöld, FGFR2, FGF8, FGF10 and BMP7 as candidate genes for hypospadias, Eur. J. Hum. Genet. 15 (2007) 405–410.
[25] S.L. Carmichael, C. Ma, S. Choudhry, E.J. Lammer, J.S. Witte, G.M. Shaw, Hypospadias and genes related to genital tubercle and early urethral development, J. Urol. 190 (2013) 1884–1892.
[26] L.S. Baskin, K. Himes, T. Colborn, Hypospadias and endocrine disruption: is there a connection? Environ. Health Perspect. 109 (2001) 1175–1183.
[27] C.M. Rocheleau, P.A. Romitti, L.K. Dennis, Pesticides and hypospadias: a meta-analysis, J. Pediatr. Urol. 5 (2009) 17–24.
[28] R.M. Sharpe, Pediatrics: endocrine disruption and human health effects–a call to action, Nat. Rev. Endocrinol. 7 (2011) 633–634.
[29] V.S. Wilson, C.R. Blystone, A.K. Hotchkiss, C.V. Rider, L.E. Gray Jr., Diverse mechanisms of anti-androgen action: impact on male rat reproductive tract development, Int. J. Androl. 31 (2008) 178–187.
[30] C.V. Rider, J.R. Furr, V.S. Wilson, L.E. Gray Jr., Cumulative effects of *in utero* administration of mixtures of reproductive toxicants that disrupt common target tissues via diverse mechanisms of toxicity, Int. J. Androl. 33 (2010) 443–462.
[31] S.L. Carmichael, J.S. Witte, C. Ma, E.J. Lammer, G.M. Shaw, Hypospadias and variants in genes related to sex hormone biosynthesis and metabolism, Andrology 2 (2014) 130–137.
[32] M.L. Gredler, A.W. Seifert, M.J. Cohn, Tissue-specific roles of Fgfr2 in development of the external genitalia, Development 142 (2015) 2203–2212.
[33] M.J. Cohn, Development of the external genitalia: conserved and divergent mechanisms of appendage patterning, Dev. Dyn. 240 (2011) 1108–1115.
[34] S.D. Blaschko, G.R. Cunha, L.S. Baskin, Molecular mechanisms of external genitalia development, Differentiation 84 (2012) 261–268.
[35] M. Harada, A. Omori, C. Nakahara, N. Nakagata, K. Akita, G. Yamada, Tissue-specific roles of FGF signaling in external genitalia development, Dev. Dyn. 244 (2015) 759–773.
[36] L.S. Baskin, A. Erol, P. Jegatheesan, Y. Li, W. Liu, G.R. Cunha, Urethral seam formation and hypospadias, Cell Tissue Res. 305 (2001) 379–387.
[37] A.W. Seifert, Z. Zheng, B.K. Ormerod, M.J. Cohn, Sonic hedgehog controls growth of external genitalia by regulating cell cycle kinetics, Nat. Commun. 1 (2010) 1–23.
[38] E.A. Morgan, S.B. Nguyen, V. Scott, H.S. Stadler, Loss of Bmp7 and Fgf8 signaling in Hoxa13-mutant mice causes hypospadia, Development 130 (2003) 3095–3109.
[39] H.S. Stadler, Modelling genitourinary defects in mice: an emerging genetic and developmental system, Nat. Rev. Genet. 4 (2003) 478–482.
[40] J. Li, E. Willingham, L.S. Baskin, Gene expression profiles in mouse urethral development, BJU Int. 98 (2006) 880–885.
[41] G. Yamada, K. Suzuki, R. Haraguchi, S. Miyagawa, Y. Satoh, M. Kamimura, N. Nakagata, H. Kataoka, A. Kuroiwa, Y. Chen, Molecular genetic cascades for external genitalia formation: an emerging organogenesis program, Dev. Dyn. 235 (2006) 1738–1752.
[42] Y. Kojima, K. Kohri, Y. Hayashi, Genetic pathway of external genitalia formation and molecular etiology of hypospadias, J. Pediatr. Urol. 6 (2010) 346–354.
[43] S.J. Sturla, A.R. Boobis, R.E. FitzGerald, J. Hoeng, R.J. Kavlock, K. Schirmer, M. Whelan, M.F. Wilks, M.C. Peitsch, Systems toxicology: from basic research to risk assessment, Chem. Res. Toxicol. 27 (2014) 314–329.
[44] Leung, M.C.K., Phuong, J., Baker, N.C., Sipes, N.S., Klinefelter, G.R., Martin, M.T., McLaurin, K.W., Setzer, R.W., Perreault, S.D., Judson, R.S., and Knudsen, T.B., Systems toxicology of male reproductive development: profiling 774 chemicals for molecular targets and adverse outcomes. Environ Health Perspect. http://ehp.niehs.nih.gov/15-10385/, http://dx.doi.org/10.1289/ehp.1510385.
[45] N.E. Skakkebaek, E. Rajpert-De Meyts, G.M. Buck Louis, J. Toppari, A.M. Andersson, M.L. Eisenberg, T.K. Jensen, N. Jørgensen, S.H. Swan, K.J. Sapra, S. Ziebe, L. Priskorn, A. Juul, Male reproductive disorders and fertility trends: influences of environment and genetic susceptibility, Physiol. Rev. 96 (2016) 55–97.
[46] A. Shirinifard, J.A. Glazier, M. Swat, J.S. Gens, F. Family, Y. Jiang, H.E. Grossniklaus, Adhesion failures determine the pattern of choroidal neovascularization in the eye: a computer simulation study, PLoS Comput. Biol. 8 (2012) e1002440.
[47] N. Kleinstreuer, D. Dix, M. Rountree, N. Baker, N. Sipes, D. Reif, R. Spencer, T. Knudsen, A computational model predicting disruption of blood vessel development, PLoS Comput. Biol. 9 (2013) e1002996.
[48] D. DeWoskin, W. Geng, A.R. Stinchcombe, D.B. Forger, It is not the parts, but how they interact that determines the behaviour of circadian rhythms across scales and organisms, Interface Focus 4 (2014) 20130076.
[49] R. Haraguchi, K. Suzuki, R. Murakami, M. Sakai, M. Kamikawa, M. Kengaku, K. Sekine, H. Kawano, S. Kato, N. Ueno, G. Yamada, Molecular analysis of external genitalia formation: the role of fibroblast growth factor (Fgf) genes during genital tubercle formation, Development 127 (2000) 2471–2479.
[50] C.L. Perriton, N. Powles, C. Chiang, M.K. Maconochie, M.J. Cohn, Sonic hedgehog signaling from the urethral epithelium controls external genital development, Dev. Biol. 247 (2002) 26–46.
[51] P.J. Hynes, J.P. Fraher, The development of the male genitourinary system. I. The origin of the urorectal septum and the formation of the perineum, Br. J. Plast. Surg. 57 (2004) 27–36.
[52] P.J. Hynes, J.P. Fraher, The development of the male genitourinary system: II. The origin and formation of the urethral plate, Br. J. Plast. Surg. 57 (2004) 112–121.
[53] C.M. Carruthers, P.M. Foster, Critical window of male reproductive tract development in rats following gestational exposure to di-n-butyl phthalate, Birth Defects Res. B Dev. Reprod. Toxicol 74 (2005) 277–285.
[54] H.M. Scott, G.R. Hutchison, M.S. Jobling, C. McKinnell, A.J. Drake, R.M. Sharpe, Relationship between androgen action in the male programming window,

fetal Sertoli cell number, and adult testis size in the rat, Endocrinology 149 (2008) 5280–5287.
[55] C.A. Shaut, C. Saneyoshi, E.A. Morgan, W.M. Knosp, D.R. Sexton, H.S. Stadler, HOXA13 directly regulates EphA6 and EphA7 expression in the genital tubercle vascular endothelia, Dev. Dyn. 236 (2007) 951–960.
[56] E. Stott, N.F. Britton, J.A. Glazier, M. Zajac, Stochastic simulation of benign avascular tumor growth using the potts model, Math. Comput. Model. 30 (1999) 183–198.
[57] N.B. Ouchi, J.A. Glazier, J.-P. Rieu, A. Upadhyaya, Y. Sawada, Improving the realism of the cellular potts model in simulations of biological cells, Physica A 329 (2003) 451–458.
[58] M.H. Swat, G.L. Thomas, J.M. Belmonte, A. Shirinifard, D. Hmeljak, J.A. Glazier, Multi-scale modeling of tissues using CompuCell3D, Methods Cell Biol. 110 (2012) 325–366.
[59] N. Metropolis, S. Ulam, The Monte Carlo method, J. Am. Stat. Assoc. 44 (1949) 335–341.
[60] S. Ray, D. Yuan, N. Dhulekar, B. Oztan, B. Yener, M. Larsen, Cell-based multi-parametric model of cleft progression during submandibular salivary gland branching morphogenesis, PLoS Comput. Biol. 9 (2013) e1003319.
[61] E. Boghaert, D.C. Radisky, C.M. Nelson, Lattice-based model of ductal carcinoma in situ suggests rules for breast cancer progression to an invasive state, PLoS Comput. Biol. 10 (2014) e1003997.
[62] Y. Satoh, R. Haraguchi, T.J. Wright, S.L. Mansour, J. Partanen, M.K. Hajihosseini, V.P. Eswarakumar, P. Lonai, G. Yamada, Regulation of external genitalia development by concerted actions of FGF ligands and FGF receptors, Anat. Embryol. (Berl.) 208 (2004) 479–486.
[63] S. Memarzadeh, L. Xin, D.J. Mulholland, A. Mansukhani, H. Wu, M.A. Teitell, O.N. Witte, Enhanced paracrine FGF10 expression promotes formation of multifocal prostate adenocarcinoma and an increase in epithelial androgen receptor, Cancer Cell 12 (2007) 572–585.
[64] E. Dessaud, A.P. McMahon, J. Briscoe, Pattern formation in the vertebrate neural tube: a sonic hedgehog morphogen-regulated transcriptional network, Development 135 (2008) 2489–2503.
[65] D. Coveney, J. Cool, T. Oliver, B. Capel, Four-dimensional analysis of vascularization during primary development of an organ, the gonad, Proc. Natl. Acad. Sci. USA. 105 (2008) 7212–7217.
[66] B. Chen, B.R. Zirkin, R. Ge, The Leydig cell as a target for toxicants Comprehensive Toxicology, 11, 2nd ed., Elsevier Ltd., Oxford, United Kingdom, 2010, pp. 131–148.
[67] R Core Team, R: A Language and Environment for Statistical Computing, R Foundation for Statistical Computing, Vienna, Austria, 2014 http://www.R-project.org/.
[68] C.M. Griffith, E.D. Hay, Epithelial-mesenchymal transformation during palatal fusion: carboxyfluorescein traces cells at light and electron microscopic levels, Development 116 (1992) 1087–1099.
[69] C. Mori, N. Nakamura, Y. Okamoto, M. Osawa, K. Shiota, Cytochemical identification of programmed cell death in the fusing fetal mouse palate by specific labelling of DNA fragmentation, Anat Embryol (Berl.) 190 (1994) 21–28.
[70] D. Sun, S. Baur, E.D. Hay, Epithelial-mesenchymal transformation is the mechanism for fusion of the craniofacial primordia involved in morphogenesis of the chicken lip, Dev. Biol. 228 (2000) 337–349.
[71] H.J. Ray, L. Niswander, Mechanisms of tissue fusion during development, Development 139 (2012) 1701–1711.
[72] Y.X. Li, H.T. Yang, M. Zdanowicz, J.K. Sicklick, Y. Qi, T.J. Camp, A.M. Diehl, Fetal alcohol exposure impairs hedgehog cholesterol modification and signaling, Lab. Invest. 87 (2007) 231–240.
[73] H.W. Kietzman, J.L. Everson, K.K. Sulik, R.J. Lipinski, The teratogenic effects of prenatal ethanol exposure are exacerbated by sonic hedgehog or GLI2 haploinsufficiency in the mouse, PLoS One 9 (2014) e89448.
[74] K.L. Howdeshell, C.V. Rider, V.S. Wilson, J.R. Furr, C.R. Lambright, L.E. Gray Jr., Dose addition models based on biologically relevant reductions in fetal testosterone accurately predict postnatal reproductive tract alterations by a phthalate mixture in rats, Toxicol. Sci. 148 (2015) 488–502.
[75] L.E. Gray Jr., J. Furr, K.R. Tatum-Gibbs, C. Lambright, H. Sampson, B.R. Hannas, V.S. Wilson, A. Hotchkiss, P.M. Foster, Establishing the 'biological relevance' of dipentyl phthalate reductions in fetal rat testosterone production and plasma and testis testosterone levels, Toxicol. Sci. 149 (2016) 178–191.
[76] T. Mammoto, A. Mammoto, Y.S. Torisawa, T. Tat, A. Gibbs, R. Derda, R. Mannix, M. de Bruijn, C.W. Yung, D. Huh, D.E. Ingber, Mechanochemical control of mesenchymal condensation and embryonic tooth organ formation, Dev. Cell. 21 (2011) 758–769.
[77] S. Memarzadeh, L. Xin, D.J. Mulholland, A. Mansukhani, H. Wu, M.A. Teitell, O.N. Witte, Enhanced paracrine FGF10 expression promotes formation of multifocal prostate adenocarcinoma and an increase in epithelial androgen receptor, Cancer Cell. 12 (2007) 572–585.
[78] J. Gibney, T. Wolthers, M. Males, G. Smythe, A.M. Umpleby, K.K.Y. Ho, Testosterone enhances the effect of growth hormone (GH) to increase IGF-I but exerts an anabolic effect that is independent of GH action, Endocrine Abstracts 5 (2003) 161.
[79] S. Miyagawa, D. Matsumaru, A. Murashima, A. Omori, Y. Satoh, R. Haraguchi, J. Motoyama, T. Iguchi, N. Nakagata, C.C. Hui, G. Yamada, The role of sonic hedgehog-Gli2 pathway in the masculinization of external genitalia, Endocrinology 152 (2011) 2894–2903.
[80] R. Haraguchi, R. Mo, C. Hui, J. Motoyama, S. Makino, T. Shiroishi, W. Gaffield, G. Yamada, Unique functions of sonic hedgehog signaling during external genitalia development, Development 128 (2001) 4241–4250.